Citation: BoneKEy Reports **4**, Article number: 664 (2015) | doi:10.1038/bonekey.2015.31

www.nature.com/bonekey

ORIGINAL ARTICLE

Predicting mouse vertebra strength with micro-computed tomography-derived finite element analysis

Jeffry S Nyman[1,2,3,4], Sasidhar Uppuganti[2], Alexander J Makowski[1,3,4], Barbara J Rowland[1,4], Alyssa R Merkel[4,5], Julie A Sterling[1,4,5,6], Todd L Bredbenner[7] and Daniel S Perrien[1,2,4,8]

[1]Department of Veterans Affairs, Tennessee Valley Healthcare System, Nashville, TN, USA. [2]Department of Orthopaedic Surgery and Rehabilitation, Vanderbilt University, Medical Center East, Nashville, TN, USA. [3]Department of Biomedical Engineering, Vanderbilt University Medical Center, Nashville, TN, USA. [4]Center for Bone Biology, Vanderbilt University Medical Center, Nashville, TN, USA. [5]Department of Medicine, Division of Clinical Pharmacology, Vanderbilt University Medical Center, Nashville, TN, USA. [6]Department of Cancer Biology, Vanderbilt University Medical Center, Nashville, TN, USA. [7]Musculoskeletal Biomechanics Section, Southwest Research Institute, San Antonio, TX, USA. [8]Vanderbilt University Institute of Imaging Sciences, Vanderbilt University Medical Center, Nashville, TN, USA.

As in clinical studies, finite element analysis (FEA) developed from computed tomography (CT) images of bones are useful in pre-clinical rodent studies assessing treatment effects on vertebral body (VB) strength. Since strength predictions from microCT-derived FEAs (μFEA) have not been validated against experimental measurements of mouse VB strength, a parametric analysis exploring material and failure definitions was performed to determine whether elastic μFEAs with linear failure criteria could reasonably assess VB strength in two studies, treatment and genetic, with differences in bone volume fraction between the control and the experimental groups. VBs were scanned with a 12-μm voxel size, and voxels were directly converted to 8-node, hexahedral elements. The coefficient of determination or R^2 between predicted VB strength and experimental VB strength, as determined from compression tests, was 62.3% for the treatment study and 85.3% for the genetic study when using a homogenous tissue modulus (E_t) of 18 GPa for all elements, a failure volume of 2%, and an equivalent failure strain of 0.007. The difference between prediction and measurement (that is, error) increased when lowering the failure volume to 0.1% or increasing it to 4%. Using inhomogeneous tissue density-specific moduli improved the R^2 between predicted and experimental strength when compared with uniform $E_t = 18$ GPa. Also, the optimum failure volume is higher for the inhomogeneous than for the homogeneous material definition. Regardless of model assumptions, μFEA can assess differences in murine VB strength between experimental groups when the expected difference in strength is at least 20%.

BoneKEy Reports **4**, Article number: 664 (2015) | doi:10.1038/bonekey.2015.31

Introduction

The use of finite element analysis (FEA) to assess the strength of bone continues to increase as high-speed processors become more affordable and commercial software to convert quantitative computed tomography (QCT) scans to finite element (FE) models and to apply relevant boundary conditions becomes more widely available. The popularity of QCT-FEA (a.k.a. homogenized FEA) is evident in the growing number of clinical studies reporting strength predictions with FEAs derived from QCT scans of the hip,[1,2] spine,[3,4] distal tibia[5,6] and distal radius.[7,8] Moreover, as evidence of their ability to make such predictions, QCT-FEAs can differentiate fracture patients from non-fracture patients, although some overlap in predicted strength exists across the cohorts.[9–14] Much of the validation behind the failure criteria in these FE model predictions came from correlations with strength measurements as determined by whole bone testing of cadaveric tissue from large animals and humans, namely the proximal femur, distal radius and vertebra,[15–19] whereas little validation has been performed on murine bone. Material assumptions are based on a number of

Correspondence: Dr JS Nyman, Department of Orthopaedic Surgery and Rehabilitation, Vanderbilt University, Medical Center East, South Tower, Suite 4200, Nashville, 37232 TN, USA.
E-mail: jeffry.s.nyman@vanderbilt.edu

Received 21 August 2014; accepted 4 February 2015; published online 22 April 2015

Table 1 Results from a linear regression analysis of experimental versus predicted strength of mouse L6 vertebrae (VB) show the effect of varying failure volume on the VB strength prediction for μFEAs using a homogeneous elastic modulus (E_t) and an inhomogeneous, element-specific E_t ($\nu = 0.03$, failure strain = 0.007, threshold of 421.4 mg HA cm^{-3})

Failure volume (%)	E_t *(GPa)*	*RMSE*[a] *(N)*	R^2 *(%)*	*Slope (95% CI)*	*Intercept (95% CI)*
0.1	18	13.3	55.2	1.82 (0.73–2.90)	−11.3 (−42.51–19.92)
0.5	18	8.2	62.9	1.68 (0.83–2.54)	−17.10 (−46.64–12.44)
1	18	5.8	66.9	1.62 (0.86–2.37)	−20.2 (−48.74–8.32)
2	18	5.0	62.3	1.38 (0.67–2.09)	−15.5 (−44.7–13.6)
3	18	5.5	62.0	1.34 (0.64–2.03)	−16.8 (−46.78–13.16)
4	18	6.3	61.9	1.31 (0.63–1.99)	−17.8 (−48.35–12.75)
10	18	11.1	61.4	1.19 (0.57–1.82)	−19.8 (−51.78–12.14)
0.1	Specific[b]	25.5	63.7	2.11 (1.06–3.17)	7.30 (−9.63–24.24)
0.5	Specific	21.3	66.0	1.84 (0.97–2.72)	3.8 (−13.94–21.60)
1	Specific	19.0	68.6	1.74 (0.96–2.52)	1.90 (−15.70–19.50)
2	Specific	16.3	70.4	1.60 (0.91–2.29)	0.55 (−16.91–18.02)
3	Specific	14.5	70.7	1.53 (0.87–2.18)	−0.38 (−18.08–17.33)
4	Specific	13.1	71.1	1.49 (0.86–2.11)	−1.46 (−19.47–16.55)
10	Specific	8.1	71.6	1.38 (0.80–1.96)	−6.1 (−25.80–13.62)
11	Specific	7.6	71.4	1.37 (0.79–1.94)	−6.54 (−26.51–13.44)
15	Specific	5.7	70.7	1.31 (0.75–1.87)	−7.87 (−28.73–12.99)
20	Specific	4.5	69.9	1.24 (0.70–1.79)	−8.57 (−30.17–13.03)

Abbreviations: CI, confidence interval; μFEA, micro-computed tomography-derived finite element analysis; RMSE, root mean squared error; VB, vertebral body.
[a]RMSE indicates how far way the regression is from the unity line. [b]Inhomogeneous material definitions based on Wagner conversion (equation 1).

published empirical relationships that either (i) convert volumetric mineral density to tissue modulus (E_t)[20] in which the attenuation in CT is converted to density using a hydroxyapatite (HA) phantom and elastic tissue modulus (E_t) is derived from local measurements by nanoindentation, (ii) relate QCT density to ash density[21] and then convert ash density to apparent-level material properties for which different empirical relationships exist for different directions of loading (compression versus tension) and bone type (cortical versus trabecular)[17,22] or (iii) relate QCT volumetric density directly to apparent-level properties using empirical relationships developed from cadaveric experiments.[23]

Mice are widely used to identify mechanisms and signaling pathways that impact bone strength because of the availability of genetic and transgenic models in this species. Bone strength predictions by micro-computed tomography (μCT)-derived FEA (μFEA) could also be useful in pre-clinical and genetic studies involving rodents because *in vivo* μCT scanners can provide relatively high-resolution FE models of bone at baseline and at follow-up time points. Thus, longitudinal changes in bone stiffness or strength can be assessed upon treatment or other experimental manipulations.[24] Moreover, μFEA of excised bones is non-destructive allowing for subsequent histological analysis. Although a number of studies involving rodents have used μFEA to determine the effect of drug treatment on bone strength,[25–30] there is little evidence in the literature establishing that μFEA can accurately predict the mechanical properties of rodent bone, and especially murine bones. Of the few studies comparing FEA predictions to experimental measurements of strength in rodent tissues, long bones were tested with limited examination of material definitions.[31–33] In effect, μFEAs of rodent bones rely on assumptions of material properties and failure criteria from the many correlation studies involving cadaveric bone from larger species.

The lack of modulus–density relationships for rodent bone is not surprising given the relatively small size of rodent bones, especially murine vertebral bodies (VBs), and the associated challenges in experimental loading protocols. Avoiding the difficulties of sample preparation for material testing of rodent bone tissue, a few FEA studies of rodent bone developed constitutive relationships using available experimental data. One study fit a nonlinear equation to a compilation of E_t and tissue mineral density (TMD) data acquired from different species and anatomical sites and using different modalities (for example, nanoindentation, tensile tests, scanning acoustic microscopy),[28] whereas another developed a linear scaling factor to determine tissue modulus from TMD based on the ratio of whole bone stiffness (determined experimentally by three-point bending of a mouse femur) to the predicted stiffness derived from a μFEA of the same bone under similar boundary conditions.[31] In addition to the uncertainty regarding material behavior assumptions and directional dependence of rodent bone, failure criteria used in μFEA have also not been rigorously tested.

Since there is a dearth of evidence establishing the accuracy of μFEA to predict the strength of mouse bone, we performed parametric analyses to determine whether elastic μFEA models with failure criteria that were linearly dependent on modulus could predict experimentally determined VB compressive strength and could detect differences in VB strength between control and treatment groups in which the drug 1D11, a transforming growth factor β (TGF-β) inhibitor, increases bone volume fraction. To investigate whether material definitions and failure criteria are consistent across two independent studies, we applied material property relationships with near-optimized failure criteria from the mouse study involving drug treatment to another mouse study involving a genetic deletion of a transcription factor important to osteoblast differentiation (that is, activating transcription factor 4 (ATF4)) and bone volume fraction.

Results

Effect of varying failure volume for homogenous material property assignment

We first investigated how failure volume affected model predictions for a homogeneous material definition, as this is the

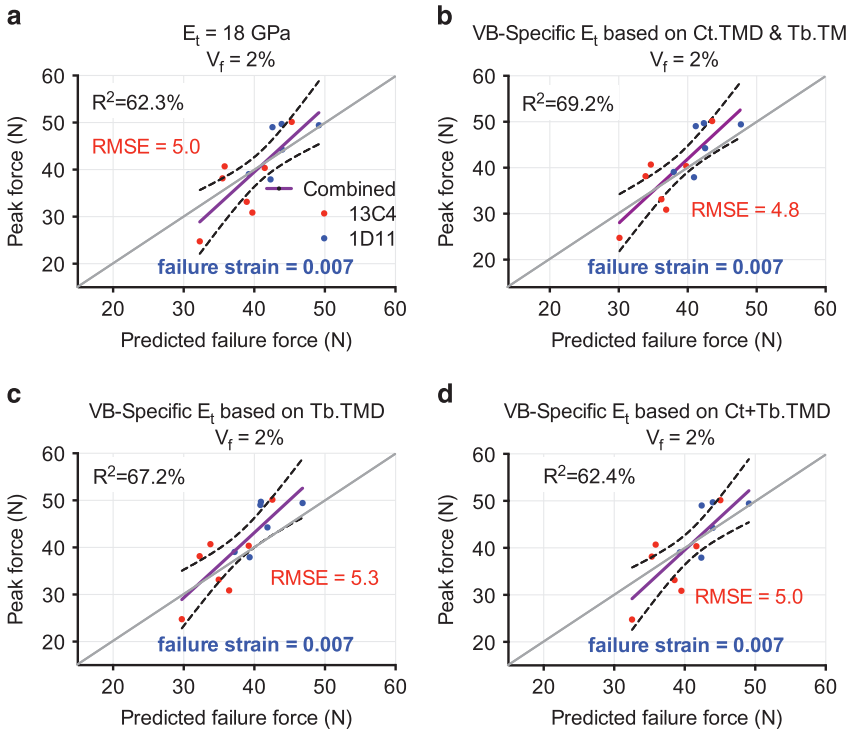

Figure 1 Linear regression analysis of experimental vertebra (VB) strength versus predicted VB strength from micro-finite element analysis (μFEAs) for different homogeneous material definitions using the same critical failure volume (V_f) and failure strain (threshold = 421.4 mg HA cm^{-3}). The prediction of VB strength had a relatively low root mean squared error (RMSE) when defining the tissue modulus (E_t) as 18 GPa for all elements in all models (**a**). Basing the tissue modulus on the mean trabecular tissue mineral density (Tb.TMD) and the mean TMD of the cortical shell (Ct.TMD), treated as two materials, increased the ability of μFEA to explain the variance in VB strength (**b**). This was also the case when basing E_t of all elements on the Tb.TMD (**c**), but not on mean Ct + Tb.TMD of the whole VB.

simplest approach to μFEA. When the modulus of all elements was set to 18 GPa and failure strain was 0.007 (Base Model), altering the failure criteria by increasing the critical failure volume (V_f) from 0.1 to 1% of total volume increased the coefficient of determination (R^2) as well as reduced the root mean squared error (RMSE) between predicted and experimental strength (**Table 1**). Additional increases in V_f did not increase the ability of the μFEA predictions to explain the variance in experimental strength. Moreover, there were nonlinear relationships between critical volume and RMSE and between critical volume and R^2 (**Table 1**).

Effects of bone compartment used to determine modulus and global threshold values

Assignment of a homogenous modulus based on the mean TMD of individual VB may improve the prediction of mechanical strength compared with using the same modulus for all VBs. However, it not clear whether VB-specific moduli should be determined from (i) the mean TMD of only trabecular bone, (ii) the mean TMD of the whole VB or (iii) whether trabecular and cortical bone should be treated as different materials with moduli corresponding to their respective mean TMDs. Using the Wagner *et al.*[34] conversion to establish a uniform VB-specific modulus based on a separate determination of mean TMD for cortical and trabecular bone (**Figure 1b**) or the mean TMD of only trabecular bone applied to the entire VB (**Figure 1c**) increased the R^2 value for the correlation with experimental strength while having minimal effects on RMSE compared with using a constant modulus of 18 GPa for all bones (**Figure 1a**). This suggests that the effect of TGF-β inhibition on bone strength is primarily via effects on trabecular bone.

Increasing the threshold to reduce the number of surface voxels in the model (that is, suppressing partial volume effect at the cost of disconnecting trabeculae) improved the ability of μFEA models with homogeneous material to predict the experimental variance in VB strength (**Table 2**), but did not have the same effect in models with inhomogeneous material. However, the higher segmentation threshold resulted in fewer elements, so μFEA models created using the higher density threshold predicted lower VB strength than the experimental values and increased RMSE (**Table 2**).

Effect of using an inhomogeneous distribution of tissue elastic modulus

Another way to account for differences in mineralization among groups is to use a heterogeneous distribution of E_t. This typically involves converting the TMD of each element to E_t using a theoretical relationship between TMD and E_t. We investigated three published conversions: Wagner *et al.*[34] (equation 1), Easley *et al.*[28] and Renders *et al.*[35] The use of an element-specific E_t to generate μFEA models improved the R^2, regardless of whether the Wagner *et al.*,[34] the Easley *et al.*[28] or the Renders *et al.*[35] relationship was used to convert TMD to E_t (**Table 1** and **Figure 2**). Keeping failure strain and failure volume set to 0.007 and 2%, respectively, results in an under-prediction of the peak force. The RSME was especially high for models developed using the Renders *et al.*[35] relationship. Simply increasing failure strain improves the accuracy (**Figure 2**) without negatively affecting predictive ability (no change in R^2 or

Table 2 Results from a linear regression analysis of experimental versus predicted strength of mouse vertebras (VBs) show the effect of global thresholding on the VB strength prediction for several FEAs using homogeneous elastic modulus (E_t) or 2 materials with $\nu = 0.3$, equivalent failure strain = 0.007 and failure volume = 2% or inhomogeneous modulus using Wagner-based conversion, $\nu = 0.3$, equivalent failure strain = 0.009, and failure volume = 6%

Threshold (mgHA cm^{-3})	E_t *(GPa)*	*RMSE (N)*	R^2 *(%)*	*Slope 95% CI*	*Intercept 95% CI*
421.4	18 GPa	5.0	62.3	1.38 (0.67–2.09)	−15.5 (−44.7–13.6)
538.9	18 GPa	8.1	70.7	1.37 (0.78–1.95)	−5.64 (−25.57–14.30)
421.4	VB specific[a]	5.3	67.2	1.38 (0.74–2.02)	−12.18 (−36.80–12.43)
538.9	VB specific	9.7	74.0	1.15 (0.70–1.61)	−4.06 (−26.61–6.62)
421.4	Element specific[b]	4.1	71.7	1.11 (0.65–1.57)	−4.26 (−23.54–14.80)
538.9	Element specific	16.7	72.9	1.09 (0.65–1.53)	−0.36 (−17.14–16.41)

Abbreviations: CI, confidence interval; RMSE, root mean squared error; VB, vertebral body.
[a]Two materials: modulus 1 determined from the mean TMD of trabecular bone and modulus 2 determined from the mean TMD of the cortical shell (both using Wagner conversion). [b]Inhomogeneous material definitions based on Wagner conversion.

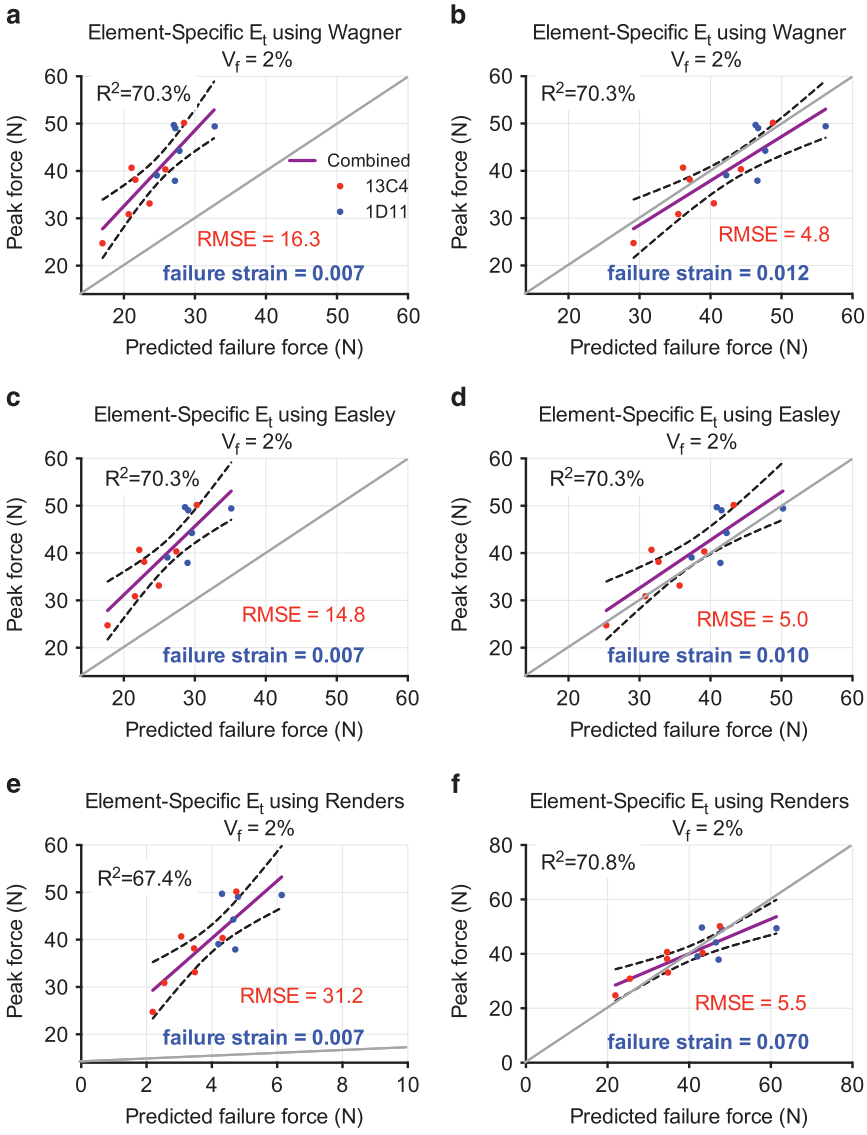

Figure 2 Linear regression analysis of experimental VB strength versus predicted VB strength for different inhomogeneous material definitions using the same critical failure volume (V_f) but different failure strains (threshold = 421.8 mg HA cm^{-3}). For a given conversion of TMD to tissue elastic modulus E_t (**a**, **c**, **e**), there was an improvement in the coefficient of determination relative to homogeneous material definitions. Increasing the failure strain decreased the error, but the failure strain required for low error varied among the different conversions (**b**, **d**, **f**).

an increase in R^2). Similarly, when failure strain was maintained at 0.007, the optimal failure volume for each inhomogeneous model was higher than for homogenous μFEA models (**Table 1**). Importantly, each relationship between E_t and TMD had different near-optimal failure criteria (maximize R^2 while minimizing RSME), and the improvement in predictive ability with optimization is small (compare **Figure 2** with Wagner: $R^2 = 71.7\%$ and RMSE = 4.1 for $V_f = 7\%$ at 0.009 failure strain; Easley: $R^2 = 71.3\%$ and RMSE = 4.1 for $V_f = 5\%$ at 0.009 failure strain and Renders: $R^2 = 70.8\%$ and RMSE = 5.5 for $V_f = 2\%$ at 0.070 failure strain).

Predictive ability of near-optimized parameters in a genetic mouse model

Building confidence in the elastic approach to predicting the strength of mouse VBs by μFEA, there was also a strong correlation between predicted and experimental strength in the study involving the genetic deletion of ATF4 with low error (**Figure 3**). Again, using inhomogeneous element-specific E_t, instead of a constant 18 GPa for all elements, increased the R^2 value, albeit marginally (**Figures 3a, b and d**).

Differences in bone volume fraction (BV/TV) and strength between experimental groups

As expected, mice treated with the TGF-β inhibitor 1D11 had greater trabecular bone volume fraction within the VB than mice treated with 13C4, the control antibody. In addition, there was lower bone volume fraction in the ATF4-deficient VBs than in VBs from wild-type littermates (**Table 3**). For both studies, the group with the lower BV/TV had lower VB compressive strength as determined experimentally and using μFEA. There were significant differences in VB strength between respective experimental groups, regardless of the material model used in generating the models (**Table 3**).

Discussion

Although there is ample evidence that CT-derived FEA models can predict the experimental strength of human bone,[36] there is little evidence that the same methods for assigning material properties in FEAs are appropriate for mouse bone. Upon comparing μFEA-derived strength to experimentally measured strength of the L6 VB from two different mouse studies, we find that an elastic FEA with linear failure criteria and relatively low computation time (<1 h) can accurately predict the compressive strength of mouse vertebrae when the FE model is generated from μCT scans using a voxel or element size of 12 μm. The accuracy of the μFEA predictions, of course, depended on the definitions of material behavior and failure criteria, but error between predicted and experimental strength values in the present study was minimal when bone was assumed to have a homogeneous tissue modulus of 18 GPa or was assigned material properties based on the Wagner *et al.*[34] conversion and failure occurred when 2% of the tissue volume exceeded 7000 μstrain (equivalent). Moreover, accounting for any possible differences in mineralization among mice, an inhomogeneous element-specific distribution of E_t provides the best explanation of the variance in experimental strength, although the optimal failure criteria differs from that of the homogeneous material definition.

Interestingly, homogeneous μFEAs models predicted a smaller difference in strength between groups than the experimental strength difference, suggesting homogeneous μFEAs may under predict experimental effects on strength. However, inhomogeneous μFEAs predicted a similar percent difference as compression tests in VB strength between 13C4- and 1D11-treatment and between *Atf4* + / + and *Atf4* − / − mice (**Table 3**). Even though the homogenous E_t and the inhomogeneous E_t models under-predicted VB strength, they still detected differences between the experimental groups.

Varying the critical failure volume for the homogeneous material definition between 1% and 4% of the total bone volume affected the coefficient of determination with modest effects on the error (**Table 1**). Using a similar FEA approach to predict the failure loads of cadaveric radii with $E_t = 10$ GPa, Pistoia *et al.*[18] also observed a small decrease in R^2, a decrease in the regression slope toward 1, and an increase in error as the failure volume was increased from 2 to 4%. In a follow-up study using the same 0.007 effective strain threshold for element failure, a nonlinear relationship was observed for critical failure volume (0.1–50% of model volume) versus the error between predicted and experimentally measured strength of embalmed human distal radii, which were scanned at a nominal resolution of 89 μm (compared with 165 μm from the previous study) with a lower tissue modulus of 6.829 GPa.[19] Like the present study involving mouse VBs, these studies found that the optimum failure volume for a homogeneous material definition was between 1 and 10%.[18,19] Conceivably, for any given study, there is an optimum failure volume and an optimum failure strain that maximizes R^2 and minimizes RMSE, respectively. However, the data presented here demonstrate that achieving this optimum is not essential to detect group-wise differences in whole-bone strength that are greater than 20% (**Table 3**).

To date, tissue-level failure strain and modulus have not been measured for mouse trabecular bone. However, nanoindentation on wet bone tissue within VBs indicates that E_t is 12.3 GPa on average for human trabecular bone[37] and ranges from 12.4 ± 0.3 GPa[38] to 20.8 ± 6.5 GPa[39] for rat trabecular bone. Note that nanoindentation involves complex loading modes (that is, not pure tension or compression) and modulus can be highly variable within a sample. In homogeneous FEA studies of VB mechanics, tissue-level elastic properties range from 8.56 GPa (ovine)[40] to 18 GPa[41] or 18.5 GPa (human).[42] In looking at the distribution of TMD among all 'bone' voxels (that is, outer voxels were not removed), E_t for 80% of elements typically varied between 5 and 19 GPa (**Figure 4**) with a mean of 17.7 GPa. Tissue modulus values in the present study are similar to previous estimates for human trabecular bone in the femoral neck based on TMD determined using synchrotron radiation,[43] and the range of nanoindentation values (4.0–19.8 GPa) measured for ovine L5 VB trabecular bone in which inhomogeneous FEAs predicted apparent compressive modulus reasonably well.[44] In contrast, the overall mean E_t is higher than E_t values calibrated by minimizing the difference between FEA results and apparent-level properties of trabecular bone cores from human tibia (2.23–10.1 GPa),[45] bovine tibia (6.77 GPa)[46] and human L2-L5 VBs (9.6 ± 1.9–13.6 ± 3.9 GPa depending on boundary conditions and element size).[47]

The assumed failure strain used here (von Mises equivalent strain = 0.007) is similar to that in previous studies simulating nonlinear force versus displacement behavior of trabecular

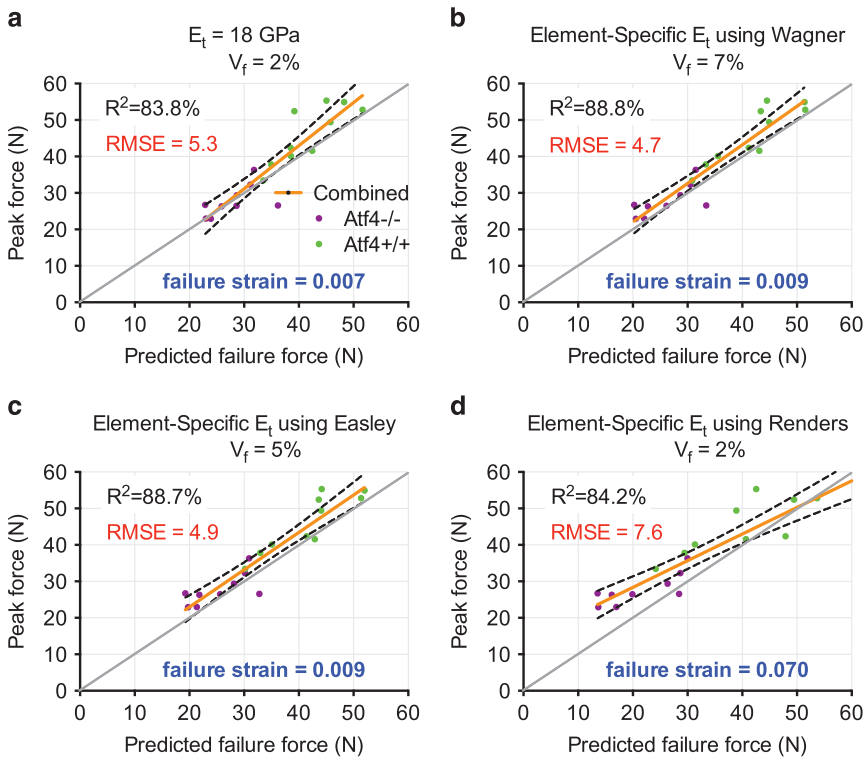

Figure 3 Linear regression analysis of experimental VB strength versus predicted VB strength for different near-optimal failure criteria and several different material definitions (threshold = 421.8 mg HA cm^{-3}) using L6 VBs from mice lacking a transcription factor (*Atf4*$^{-/-}$) and wild-type littermates (*Atf4*$^{+/+}$). The μFEA-predicted strength strongly correlated with experimental strength whether all elements (**a**) had a modulus of 18 GPa, (**b**) had an inhomogeneous modulus based on several published conversions (**b**, **c**, **d**).

Table 3 Differences in selected properties of VBs between the experimental groups as assessed by μCT, compression testing and μFEM using equivalent failure strain = 0.7%, and failure volume = 2% for the homogeneous models and near-optimized parameters for the inhomogeneous, element-specific models

Property	*TGF-β inhibition study*				*Activation transcription factor 4 study*			
	13C4 (n = 7)	*1D11* (n = 8)	*% Diff*	P-*value*	*Atf4*$^{+/+}$ (n = 10)	*Atf4*$^{-/-}$ (n = 10)	*% Diff*	P-*value*
BV/TV	0.261 ± 0.032	0.315 ± 0.019	19.0	0.001	0.148 ± 0.011	0.102 ± 0.022	36.9	0.0001
Tb.TMD	970 ± 14	982 ± 9	1.3	0.058	1035 ± 13	1032 ± 13	0.3	0.57
Peak force (N)[a]	36.9 ± 8.2	44.9 ± 5.4	19.6	0.065	46.0 ± 7.9	27.8 ± 4.3	49.5	0.0001
Predicted strength (N)								
E_t = 10 GPa	21.4 ± 2.4	23.9 ± 1.7	11.4	0.030	23.2 ± 3.3	15.6 ± 2.4	32.8	0.0001
E_t = 18 GPa	38.4 ± 4.3	43.1 ± 3.0	11.4	0.030	41.8 ± 5.9	28.1 ± 4.3	32.8	0.0001
VB specific E_t[b]	36.4 ± 4.3	41.2 ± 3.7	12.9	0.040	37.9 ± 5.5	30.5 ± 8.9	24.0	0.0001
Tissue-specific E_t[c]	37.0 ± 5.6	44.0 ± 3.4	18.8	0.011	42.0 ± 7.0	26.5 ± 4.8	36.9	0.0001
Tissue-specific E_t[d]	36.6 ± 6.0	44.2 ± 3.7	20.8	0.010	41.8 ± 7.2	25.8 ± 5.0	38.2	0.0001
Tissue-specific E_t[e]	34.6 ± 9.0	47.5 ± 6.0	37.4	0.006	42.1 ± 11.7	21.9 ± 6.5	47.9	0.0002

Abbreviations: μCT, micro-computed tomography; μFEA, micro-finite element analysis; Diff, difference; Tb.TMD, trabecular tissue mineral density; VB, vertebral body. [a]*n* = 6 for 1D11 and n = 9 for *Atf4*$^{-/-}$ in the compression tests. [b]Two materials: one for trabecular bone and the other for the cortical shell using Wagner conversion. [c]Wagner: linear approximation of (equation 1) E_t = -6034 + 23.434 × TMD (**Figure 7**); Easley. [d]$E_t = 0.1127 \times TMD^{1.746}$. [e]Renders: $E_t = 3.883 \times 10^{-9} \times TMD^{4.05}$.

bone cores,[46,48] but true failure strain of individual trabeculae can be highly variable.[49] In a nonlinear μFEA incorporating damage, the strains at which damage forms in trabeculae were determined to be − 0.0116 (compression) and 0.0069 (tension) when the model was calibrated against compression tests of ovine trabecular bone.[50] The corresponding fracture strain estimates were double the damage strains, and so a failure strain between 0.02 and 0.007 appears reasonable. This range could not be achieved for the Renders *et al.*[35] relationship when the failure volume was less than 10%. Despite the uncertainty in material behavior and failure conditions of mouse trabecular bone, applying constant properties and failure criteria across all models can still predict VB strength with reasonable accuracy, at least in situations where BV/TV and TMD drive differences in VB strength.

Using element-specific E_t improves the ability of μFEA models to explain the variance in VB strength, at least when using an inhibitor of TGF-β, which affects TMD. Similarly, previous studies have reported improvements in predicting porcine VB strength,[51] apparent modulus of human trabecular

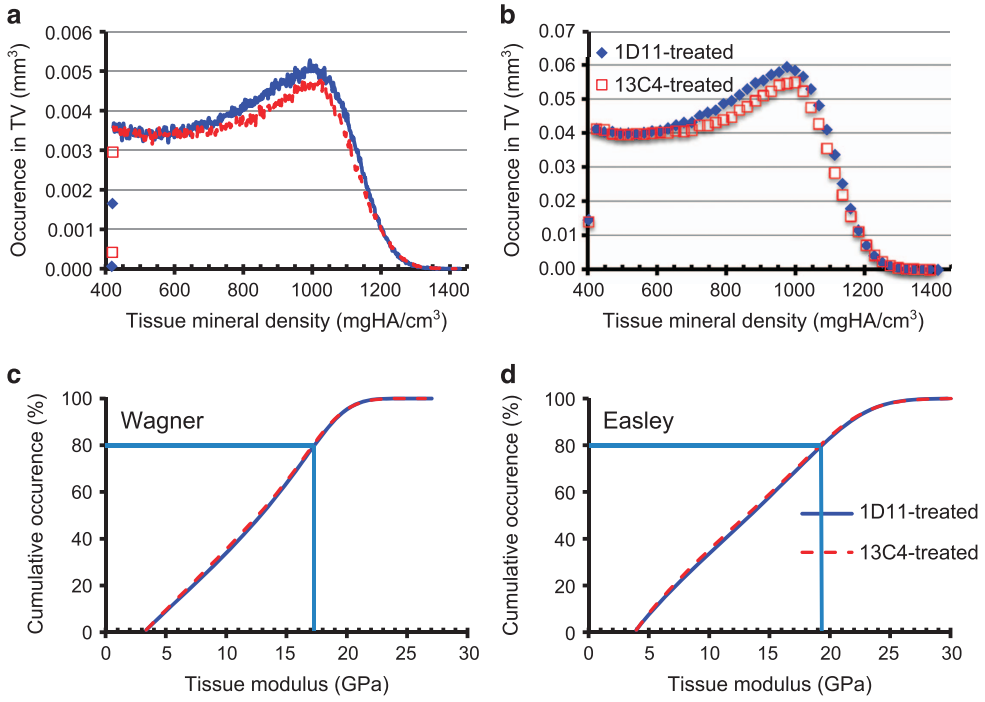

Figure 4 When solving the inhomogeneous μFEAs, the range of TMD values (**a**) was divided into larger bins, resulting in approximately 42 unique materials (**b**). When plotted as the cumulative occurrence of the percent total volume (TV) for the same representative histograms, element-specific E_t is between 5 and 19 (**c**) or 22 GPa (**d**) for 80% of the elements depending on which conversion was used (Wagner or Easley).

bone[52] and compressive strength of the distal radius from cadavers[53] when changing from homogeneous modulus to an inhomogeneous, element- or tissue-specific modulus. The decrease in predicted force with the use of inhomogeneous distribution of E_t (**Figure 3**) is consistent with observed decreases in predicted apparent modulus of human trabecular bone when using inhomogeneous FEAs.[35,52] That is, for a given apparent displacement of trabecular bone or VB, local stresses are lower and higher in regions of lower and higher tissue modulus, respectively. The net decrease in modulus when changing from the homogeneous (18 GPa) model to the inhomogeneous model leads to a decrease in the reaction force. Under-prediction of VB strength (loss of accuracy) was corrected in elastic FEA models by increasing failure strain or increasing the failure volume.

Whether nonlinear μFEAs would further improve mouse VB strength predictions is not known at this time. Certainly, nonlinear analysis (for example, elastic-perfectly plastic constitutive models) has been useful in continuum-level homogenized FEAs in which low image resolution prevents explicit description of trabecular microstructure.[54] However, such analysis would require substantially more computational time. Another limitation of the present study is that the small size and irregular shape of the mouse VB prevented accurate measurements of displacement and identification of the yield point. Thus, we could not compare stiffness or yield force as determined from μFEA models to corresponding experimentally determined values. Moreover, potting the cranial-caudal ends to match boundary conditions of the μFEAs is exceedingly difficulty and so the roughened platens were assumed to provide sufficient friction to match the boundary conditions of the μFEA models. Additional improvements in VB strength prediction may also be achieved with different failure criteria (for example, based on strain energy density), different boundary conditions (for example, low friction) and use of μCT scans after the endplates and transverse processes (TPs) have been removed. Regardless, there are relatively strong correlations between predicted and experimental VB strength with isotropic, linear material assumptions with node displacement restricted in the transverse directions at the caudal end. The present correlations are perhaps not as strong as those obtained from human bone testing, but again, the size of mouse VB is likely to introduce artifacts in experimental testing that are not present in testing of larger bones. In addition, R^2 values from the present μFEA models are comparable to those obtained comparing predictions of QCT-FEAs ($R^2 = 72\%$) to the results from compression tests of cadaveric, lumbar VBs.[54]

The improvement in R^2 with an increase in global segmentation threshold (**Table 2**) is similar to the improvement gained with an inhomogeneous E_t. Many elements with lower modulus values ($E_t = 3$–6 GPa) were near the surface, so effectively, an inhomogeneous distribution reduced effective bone volume, as did the application of higher density threshold, which eliminated lower density surface voxels (**Figure 5**). We also observed a slight discrepancy in predicted failure force between fe_solve3 and fe_solveD, the built-in Scanco FEA solvers, when 18 GPa was assigned to all elements. This is likely due to the error tolerance used (1×10^{-4}) for solution convergence by the elastic solver and propagation of this error to calculations of failure force. However, discrepancies in the predicted failure forces for the individual VB's did not significantly alter the R^2 or RMSE values between the data sets produced from each solver. Lastly, models with lower mesh density (that is, $12 \times 12 \times 12\ \mu m^3$ elements) over-predict VB

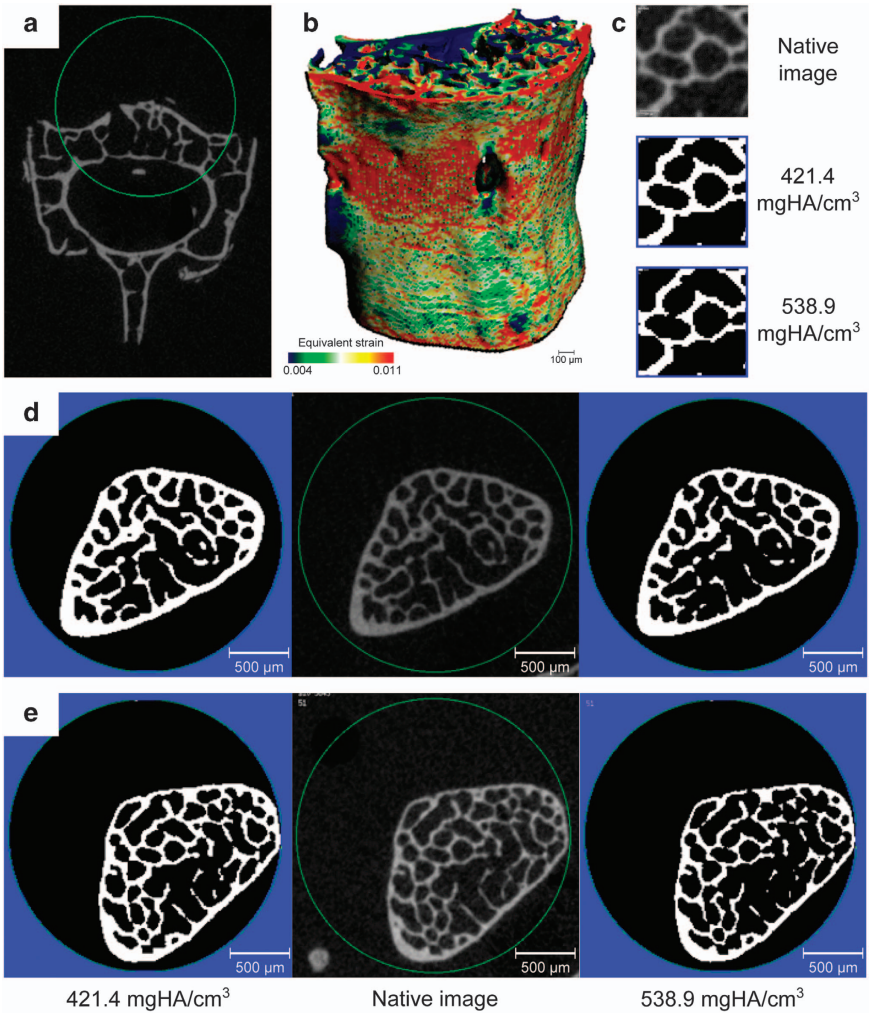

Figure 5 A circle contour of constant radius transected the non-loading bearing elements of the vertebra (**a**) to generate the three-dimensional models for finite element analysis using compression boundary conditions in which the caudal nodes were fixed in the *x*-, *y*- and *z*-direction (high friction) and cranial nodes were fixed in the *x*- and *y*-direction (high friction) with displacement in the negative *z*-direction to impart 1% apparent strain (**b**). A zoomed-in images of the trabeculae gives an indication of the mesh density for the different thresholds (**c**). Segmented images for the two thresholds are compared with the native image for the anti-TGF-β study (**d**) and the genetic ATF4 study (**e**).

strength when compared with models with a higher mesh density (that is, $6.0 \times 6.0 \times 6.0\,\mu m^3$ elements) created from μCT with constant resolution. However, the strength predictions for the two mesh densities are highly correlated, so the predictive ability does not necessarily improve with a higher mesh density while the computational time significantly increases.

Given that the near optimal failure criteria were determined for the TGF-β study, the predictive ability of elastic μFEA models, regardless of material definition, was surprisingly better for the ATF4 study. This is partly due to the larger range in strength values and smaller overlap in strength in the experimental groups for the ATF4 study than for the TGF-β-inhibitor study. Still, this does indicate that non-mineral factors could be contributing to the strength differences between control and anti-TGF-β treatments. The present work did not investigate whether other mouse models will necessarily adhere to the E_t versus TMD conversions or failure criteria used here. Nonetheless, it can serve as a benchmark for what can be expected when comparing predicted strength values to experimental strength measurements of mouse VBs.

Materials and Methods

Tissue source

L6 VBs were collected from two different mouse studies in which trabecular bone volume fraction (BV/TV) was expected to vary based on previous work.[55,56] In the first mouse study, 13-week-old male mice (FVB strain) were treated with either a TGF-β-neutralizing antibody (1D11, $n = 8$) or a control antibody (13C4, $n = 7$) for 4 weeks at the same dose ($10\,mg\,kg^{-1}$ 3x per week) because inhibiting TGF-β increases BV/TV[57] and, hence, would be expected to increase VB compressive strength. In the second study, activating transcription factor 4-null (*Atf4*$^{-/-}$) mice ($n = 10$) and their wild-type littermates ($n = 10$) were euthanized at 17 weeks of age (male and female on a FVB background). *Atf4*$^{-/-}$ mice have an extremely low bone volume phenotype,[55] and hence, their VBs should be weaker than *Atf4*$^{+/+}$ mice. Bones were stored at –20 °C in phosphate buffered saline when not being analyzed.

Micro-computed tomography FEA

Prior to mechanical testing, the VB cranial-caudal axis was aligned with the z-axis of the specimen tube holder for the

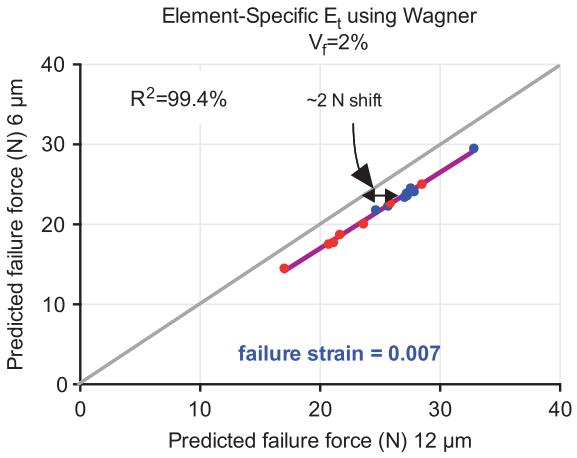

Figure 6 Linear regression analysis of predicted VB strength from a high mesh density model ($6.0 \times 6.0 \times 6.0\ \mu m^3$ brick element) versus predicted VB strength from a low mesh density model ($12 \times 12 \times 12\ \mu m^3$ brick element). The µFEAs derived from the 12-µm isotropic voxel scan under predicted strength by 2 N, but the strength predictions were highly correlated with those from the high mesh density model (threshold = 421.8 mg HA cm^{-3}).

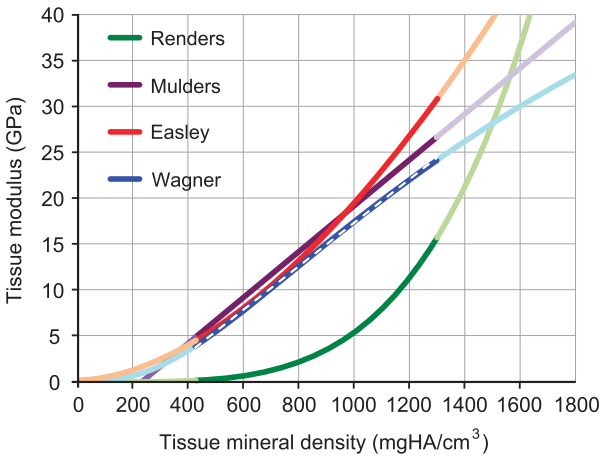

Figure 7 Of the published relationships to convert µCT-derived volumetric density to elastic modulus, this study used those derived by Wagner *et al.*[32], Easley *et al.*[28] and Renders *et al.*[35] The typical TMD range for this study is highlighted with the darker colors. A linear regression equation derived from the Wagner relationship (dashed white line) was used to calculate element-specific E_t in the inhomogeneous µFEAs.

scanner. Each L6 VB was scanned (µCT40, Scanco Medical AG, Brüttisellen, Switzerland) at an isotropic voxel size of 12 µm (70 kVp, 114 µA; 1000 projects per 360° rotation; and 300 ms integration time) and using a HA phantom calibration to determine TMD throughout the VB and the manufacturer's beam hardening correction during image reconstruction. After the raw image stack was reconstructed, the scans were loaded into Scanco µCT evaluation software and checked for alignment of the specimen axes with scan axes. If the scan was tilted from the long axis by greater than 3°, specimen orientation was corrected by rotating the image data about the *Y* and *X*-axes, respectively, using a custom script written in the Image Processing Language (IPL v5.15) for Scanco Medical AG. To specify the volume of interest used to create three-dimensional reconstructions of the vertebrae, a circle with a constant radius of 1.24 mm was copied into each image between the end plates and positioned to transect the TPs, which did not bear load in the compression test (**Figure 1a**). Recently, Boyd *et al.*[29] showed that removing the TPs from FE models did not affect relative differences in rat VB strength predictions. Vertebral endplates were not included in the model. Image noise was reduced using a Gaussian filter with a sigma of 0.3 and support of 1. Native (gray-scale) images with the noise filter were compared with segmented images across multiple VBs arriving at a global segmentation threshold of 421.4 mg HA cm^{-3} (**Figure 5**).

Scanco FE-software (fe_solve3, v1.13, Scanco Medical AG, Brüttisellen, Switzerland) was used to directly convert voxels to 8-node brick elements and element-wise strain values were determined for simulated high-friction, axial compression loading of each VB to a peak level of 1% apparent strain. That is, the caudal nodes were constrained in the *x*-, *y*- and *z*-direction, and the cranial nodes were constrained in *x*- and *y*-direction with a defined negative displacement in the z-direction. In the Base Model, all elements were assigned a homogenous elastic modulus of the bone tissue (E_t) and Poisson's ratio (ν) was 18 GPa and 0.3, respectively, for the VBs from the 1D11 study. Reaction force at failure was determined at the point in which 2% of the model volume exceeded von Mises equivalent strain of 0.007. This failure criterion was found to predict failure force values that were strongly correlated with experimental failure forces of cadaveric radii[18] and is commonly used in µFEA studies of mouse bone.[29,30] The FE models had between 676 000 and 989 000 elements with 901 000 to 1 253 000 nodes requiring a wall-clock time between 23 min and 48 min to solve and perform all post-processing on an HP BL870c system with two quad-core GHz Intel Itanium processors and 32 GB of RAM per blade server. To verify that the mesh density associated with 12 µm isotropic voxels did not inadvertently affect the predictive ability of the analyses, each element in FE models was divided into eight elements ($6.0 \times 6.0 \times 6.0\ \mu m^3$), and the µFEA models were re-run with an inhomogeneous material definition (described in the next section). The predicted failure forces for the higher mesh density strongly correlated with those for the lower mesh density with regression line nearly parallel to the unity line (**Figure 6**). Moreover, the predictive ability of the µFEAs did not improve with the higher mesh density ($R^2 = 67.7\%$ versus $R^2 = 70.4\%$ for lower mesh density). The computational time, however, significantly increased (between 8 and 14 h).

Parametric study design

A homogenous modulus ($E_t = 18$ GPa) was assigned for elements in all VB models, and the percentage of elements (V_f) that must exceed 0.007 equivalent strain before failure was varied from 0.1 to 10%. V_f was also varied from 0.1 to 20% for an inhomogeneous material property assignment (described below). Then, instead of maintaining a constant value for E_t across all VBs, a unique modulus was calculated for each VB based on mean TMD (that is, VB-specific) using a conversion derived by Wagner *et al.*[34] (see **Figure 7** with respect to other published conversions):

$$E_t = 10^A \quad \text{(GPa)} \tag{1}$$

where

$$A = -8.58 + 4.05 \times log_{10}(B)$$

and

$$B = 400/(1 + 0.504/TMD) \quad (\mathrm{gHA/cm^3})$$

There were three VB-specific material definitions: (i) E_t based on mean TMD of only the trabecular bone (Tb), (ii) E_t based on the mean TMD of the whole VB (Ct and Tb combined) and (iii) two materials with distinct E_t for trabecular and cortical bone based on the respective mean Tb.TMD and the mean Ct.TMD. Mean TMD values were determined using a standard Scanco evaluation script for all voxels remaining after the two outermost voxel layers were removed.

We also investigated whether an inhomogeneous distribution of E_t (element-specific E_t) based on individual voxel density improved μFEA predictions (fe_solveD, v1.13, Scanco Medical AG, Brüttisellen, Switzerland). In doing so, TMD distribution was binned into 43–47 materials starting at 401.21 mg HA cm^{-3} and incrementing by 22.96 mg HA cm^{-3} until reaching the maximum TMD for the given scan (**Figure 7**). The mean material density of each bin was converted to E_t using either a first-order approximation of the relationship from Wagner *et al.*[34] in the typical TMD range (420.1–1298.2 mg HA cm^{-3}; $E_t = -6034.6 + 23.4 \times$ TMD; MPa from mgHA cm^{-3}) or using the relationship from Easley *et al.*[28] ($E_t = 0.1127 \times \mathrm{TMD}^{1.746}$; MPa from mgHA cm^{-3}) or using the relationship from Renders *et al.* ($E_t = 3.883\mathrm{x}10^{-9} \times \mathrm{TMD}^{4.05}$ fits $^{10}\log \mathrm{Et} = -8.58 + 3.05 \times {}^{10}\log[\mathrm{Ca}]$ where $[\mathrm{Ca}] = 0.4\mathrm{xTMD}/2$; MPa from mgHA cm^{-3}; **Figure 7**). Initially, the failure criteria of the Base Model were used in the inhomogeneous μFEAs, and then near optimal values were sought.

To investigate the effect of setting a global threshold that lowers the number of elements, we ran a μFEA following segmentation of bone tissue with a threshold of 538.9 mg HA cm^{-3}. This higher threshold created apparent perforations or disconnections in some of the thinner trabeculae (**Figure 5**).

To verify the applicability of the failure criteria and material assumptions across studies, the strength of VBs from the wild-type and ATF4-deficient mice were determined for a subset of model parameters.

Compression tests

After gently scraping away the VB endplates with a scalpel and trimming the TPs with surgical scissors, each hydrated VB was subjected to axial compression to failure at 3 mm min^{-1} (Dynamight 8841, Instron, Norwood, MA, USA), in which the supporting platen had a rough surface and a moment relief to approximate the fixed boundary conditions in the μFEA models and off-axis loading, respectively. Upon review of high-speed video (Canon E6) recordings of the tests, the strength measurements of 2 VBs from the 1D11 study were removed from statistical analysis due to specimen slippage during compression.

Statistical analysis

The ability of μFEA to predict mouse VB strength was ascertained by linear regression to determine the intercept and slope including 95% confidence interval and the RMSE between experimentally measured peak force versus the predicted failure force of each VB. Differences in properties between experimental groups were tested for statistical significance using Student's *t*-test (two-tail) unless the data from one of the groups did not pass the Shapiro–Wilk normality test, in which case, the Mann–Whitney test was used instead. All analyses were performed with GraphPad Prism (v6.0a, GraphPad Softwared, Inc., La Jolla, CA, USA).

Conflict of Interest

The authors declare no conflict of interest.

Acknowledgements

A Concept Award from the USAMRMC (W81XWH-11-1-0628) and grants from VA BLR&D (Merit Award 1I01BX001018 and Career Development Award IK2BX001634) and NIH/NIAMS (1R01AR063157) supported this work. The micro-computed tomography scanner was supported by NIH/NCRR (1S10RR027631) and matching funds from the Vanderbilt Office of Research supported this work. We thank the Genzyme Corporation, a Sanofi Company, for donating the antibodies.

References

1. Keaveny TM, Hoffmann PF, Singh M, Palermo L, Bilezikian JP, Greenspan SL *et al.* Femoral bone strength and its relation to cortical and trabecular changes after treatment with PTH, alendronate, and their combination as assessed by finite element analysis of quantitative CT scans. *J Bone Miner Res* 2008; **23**: 1974–1982.
2. Cosman F, Keaveny TM, Kopperdahl D, Wermers RA, Wan X, Krohn KD *et al.* Hip and spine strength effects of adding versus switching to teriparatide in postmenopausal women with osteoporosis treated with prior alendronate or raloxifene. *J Bone Miner Res* 2013; **28**: 1328–1336.
3. Imai K, Ohnishi I, Yamamoto S, Nakamura K. *In vivo* assessment of lumbar vertebral strength in elderly women using computed tomography-based nonlinear finite element model. *Spine* 2008; **33**: 27–32.
4. Brixen K, Chapurlat R, Cheung AM, Keaveny TM, Fuerst T, Engelke K *et al.* Bone density, turnover, and estimated strength in postmenopausal women treated with odanacatib: a randomized trial. *J Clin Endocrinol Metab* 2013; **98**: 571–580.
5. Burghardt AJ, Kazakia GJ, Sode M, de Papp AE, Link TM, Majumdar S. A longitudinal HR-pQCT study of alendronate treatment in postmenopausal women with low bone density: Relations among density, cortical and trabecular microarchitecture, biomechanics, and bone turnover. *J Bone Miner Res* 2010; **25**: 2558–2571.
6. Lawson EA, Ackerman KE, Estella NM, Guereca G, Pierce L, Sluss PM *et al.* Nocturnal oxytocin secretion is lower in amenorrheic athletes than nonathletes and associated with bone microarchitecture and finite element analysis parameters. *Eur J Endocrinol* 2013; **168**: 457–464.
7. Kazakia GJ, Burghardt AJ, Link TM, Majumdar S. Variations in morphological and biomechanical indices at the distal radius in subjects with identical BMD. *J Biomech* 2011; **44**: 257–266.
8. Faje AT, Karim L, Taylor A, Lee H, Miller KK, Mendes N *et al.* Adolescent Girls With Anorexia Nervosa Have Impaired Cortical and Trabecular Microarchitecture and Lower Estimated Bone Strength at the Distal Radius. *J Clin Endocrinol Metab* 2013; **98**: 1923–1929.
9. Imai K, Ohnishi I, Matsumoto T, Yamamoto S, Nakamura K. Assessment of vertebral fracture risk and therapeutic effects of alendronate in postmenopausal women using a quantitative computed tomography-based nonlinear finite element method. *Osteoporos Int* 2009; **20**: 801–810.
10. Orwoll ES, Marshall LM, Nielson CM, Cummings SR, Lapidus J, Cauley JA *et al.* Finite element analysis of the proximal femur and hip fracture risk in older men. *J Bone Miner Res* 2009; **24**: 475–483.
11. Vilayphiou N, Boutroy S, Szulc P, van Rietbergen B, Munoz F, Delmas PD *et al.* Finite element analysis performed on radius and tibia HR-pQCT images and fragility fractures at all sites in men. *J Bone Miner Res* 2010; **26**: 965–973.
12. Nishiyama KK, Macdonald HM, Hanley DA, Boyd SK. Women with previous fragility fractures can be classified based on bone microarchitecture and finite element analysis measured with HR-pQCT. *Osteoporos Int* 2012; **24**: 1733–1740.
13. Graeff C, Marin F, Petto H, Kayser O, Reisinger A, Peña J *et al.* High resolution quantitative computed tomography-based assessment of trabecular microstructure and strength estimates by finite-element analysis of the spine, but not DXA, reflects vertebral fracture status in men with glucocorticoid-induced osteoporosis. *Bone* 2013; **52**: 568–577.
14. Melton LJ, Riggs BL, van Lenthe GH, Achenbach SJ, Müller R, Bouxsein ML *et al.* Contribution of in vivo structural measurements and load/strength ratios to the determination of forearm fracture risk in postmenopausal women. *J Bone Miner Res* 2007; **22**: 1442–1448.
15. Lengsfeld M, Schmitt J, Alter P, Kaminsky J, Leppek R. Comparison of geometry-based and CT voxel-based finite element modelling and experimental validation. *Med Eng Phys* 1998; **20**: 515–522.

16. Cody DD, Gross GJ, Hou FJ, Spencer HJ, Goldstein SA, Fyhrie DP. Femoral strength is better predicted by finite element models than QCT and DXA. *J Biomech* 1999; **32**: 1013–1020.
17. Keyak JH, Rossi SA, Jones KA, Skinner HB. Prediction of femoral fracture load using automated finite element modeling. *J Biomech* 1998; **31**: 125–133.
18. Pistoia W, van Rietbergen B, Lochmüller E-M, Lill CA, Eckstein F, Rüegsegger P. Estimation of distal radius failure load with micro-finite element analysis models based on three-dimensional peripheral quantitative computed tomography images. *Bone* 2002; **30**: 842–848.
19. Mueller TL, Christen D, Sandercott S, Boyd SK, van Rietbergen B, Eckstein F *et al.* Computational finite element bone mechanics accurately predicts mechanical competence in the human radius of an elderly population. *Bone* 2011; **48**: 1232–1238.
20. Mulder L, Koolstra JH, Toonder den JMJ, van Eijden TMGJ. Intratrabecular distribution of tissue stiffness and mineralization in developing trabecular bone. *Bone* 2007; **41**: 256–265.
21. Les CM, Keyak JH, Stover SM, Taylor KT, Kaneps AJ. Estimation of material properties in the equine metacarpus with use of quantitative computed tomography. *J Orthop Res* 1994; **12**: 822–833.
22. Keaveny TM, McClung MR, Wan X, Kopperdahl DL, Mitlak BH, Krohn K. Femoral strength in osteoporotic women treated with teriparatide or alendronate. *Bone* 2012; **50**: 165–170.
23. Kopperdahl DL, Morgan EF, Keaveny TM. Quantitative computed tomography estimates of the mechanical properties of human vertebral trabecular bone. *J Orthop Res* 2002; **20**: 801–805.
24. Lambers FM, Kuhn G, Schulte FA, Koch K, Müller R. Longitudinal assessment of *in vivo* bone dynamics in a mouse tail model of postmenopausal osteoporosis. *Calcif Tissue Int* 2012; **90**: 108–119.
25. Ito M, Nishida A, Aoyagi K, Uetani M, Hayashi K, Kawase M. Effects of risedronate on trabecular microstructure and biomechanical properties in ovariectomized rat tibia. *Osteoporos Int* 2005; **16**: 1042–1048.
26. Ito M, Nakayama K, Konaka A, Sakata K, Ikeda K, Maruyama T. Effects of a prostaglandin EP4 agonist, ONO-4819, and risedronate on trabecular microstructure and bone strength in mature ovariectomized rats. *Bone* 2006; **39**: 453–459.
27. Perrien DS, Akel NS, Edwards PK, Carver AA, Bendre MS, Swain FL *et al.* Inhibin A is an endocrine stimulator of bone mass and strength. *Endocrinology* 2007; **148**: 1654–1665.
28. Easley SK, Jekir MG, Burghardt AJ, Li M, Keaveny TM. Contribution of the intra-specimen variations in tissue mineralization to PTH- and raloxifene-induced changes in stiffness of rat vertebrae. *Bone* 2010; **46**: 1162–1169.
29. Boyd SK, Szabo E, Ammann P. Increased bone strength is associated with improved bone microarchitecture in intact female rats treated with strontium ranelate: a finite element analysis study. *Bone* 2011; **48**: 1109–1116.
30. Spatz JM, Ellman R, Cloutier AM, Louis L, van Vliet M, Suva LJ *et al.* Sclerostin antibody inhibits skeletal deterioration due to reduced mechanical loading. *J Bone Miner Res* 2013; **28**: 865–874.
31. Mann KA, Lee J, Arrington SA, Damron TA, Allen MJ. Predicting distal femur bone strength in a murine model of tumor osteolysis. *Clin Orthop Relat Res* 2008; **466**: 1271–1278.
32. Wernle JD, Damron TA, Allen MJ, Mann KA. Local irradiation alters bone morphology and increases bone fragility in a mouse model. *J Biomech* 2010; **43**: 2738–2746.
33. Ascenzi M-G, Lutz A, Du X, Klimecky L, Kawas N, Hourany T *et al.* Hyperlipidemia affects multiscale structure and strength of murine femur. *J Biomech* 2014; **47**: 2436–2443.
34. Wagner DW, Lindsey DP, Beaupre GS. Deriving tissue density and elastic modulus from microCT bone scans. *Bone* 2011; **49**: 931–938.
35. Renders GAP, Mulder L, Langenbach GEJ, van Ruijven LJ, van Eijden TMGJ. Biomechanical effect of mineral heterogeneity in trabecular bone. *J Biomech* 2008; **41**: 2793–2798.
36. Engelke K, Libanati C, Fuerst T, Zysset P, Genant HK. Advanced CT based *in vivo* methods for the assessment of bone density, structure, and strength. *Curr Osteoporos Rep* 2013; **11**: 246–255.
37. Wolfram U, Wilke H-J, Zysset PK. Valid micro finite element models of vertebral trabecular bone can be obtained using tissue properties measured with nanoindentation under wet conditions. *J Biomech* 2010; **43**: 1731–1737.
38. Ammann P, Badoud I, Barraud S, Dayer R, Rizzoli R. Strontium ranelate treatment improves trabecular and cortical intrinsic bone tissue quality, a determinant of bone strength. *J Bone Miner Res* 2007; **22**: 1419–1425.
39. Kim D-G, Huja SS, Navalgund A, D'Atri A, Tee B, Reeder S *et al.* Effect of estrogen deficiency on regional variation of a viscoelastic tissue property of bone. *J Biomech* 2013; **46**: 110–115.
40. Harrison NM, McHugh PE. Comparison of trabecular bone behavior in core and whole bone samples using high-resolution modeling of a vertebral body. *Biomech Model Mechanobiol* 2010; **9**: 469–480.
41. Homminga J, van Rietbergen B, Lochmüller E-M, Weinans H, Eckstein F, Huiskes R. The osteoporotic vertebral structure is well adapted to the loads of daily life, but not to infrequent 'error' loads. *Bone* 2004; **34**: 510–516.
42. Eswaran SK, Gupta A, Adams MF, Keaveny TM. Cortical and trabecular load sharing in the human vertebral body. *J Bone Miner Res* 2006; **21**: 307–314.
43. Gross T, Pahr DH, Peyrin F, Zysset PK. Mineral heterogeneity has a minor influence on the apparent elastic properties of human cancellous bone: a SRμCT-based finite element study. *Comput Methods Biomech Biomed Engin* 2012; **15**: 1137–1144.
44. Harrison NM, McDonnell PF, O'Mahoney DC, Kennedy OD, O'Brien FJ, McHugh PE. Heterogeneous linear elastic trabecular bone modelling using micro-CT attenuation data and experimentally measured heterogeneous tissue properties. *J Biomech* 2008; **41**: 2589–2596.
45. van Rietbergen B, Weinans H, Huiskes R, Odgaard A. A new method to determine trabecular bone elastic properties and loading using micromechanical finite-element models. *J Biomech* 1995; **28**: 69–81.
46. Verhulp E, van Rietbergen B, Müller R, Huiskes R. Micro-finite element simulation of trabecular-bone post-yield behaviour--effects of material model, element size and type. *Comput Methods Biomech Biomed Engin* 2008; **11**: 389–395.
47. Bevill G, Eswaran SK, Farahmand F, Keaveny TM. The influence of boundary conditions and loading mode on high-resolution finite element-computed trabecular tissue properties. *Bone* 2009; **44**: 573–578.
48. Niebur GL, Feldstein MJ, Yuen JC, Chen TJ, Keaveny TM. High-resolution finite element models with tissue strength asymmetry accurately predict failure of trabecular bone. *J Biomech* 2000; **33**: 1575–1583.
49. Hernandez CJ, Tang SY, Baumbach BM, Hwu PB, Sakkee AN, van der Ham F *et al.* Trabecular microfracture and the influence of pyridinium and non-enzymatic glycation-mediated collagen cross-links. *Bone* 2005; **37**: 825–832.
50. Harrison NM, McDonnell P, Mullins L, Wilson N, O'Mahoney D, McHugh PE. Failure modelling of trabecular bone using a non-linear combined damage and fracture voxel finite element approach. *Biomech Model Mechanobiol* 2013; **12**: 225–241.
51. Wilcox RK. The influence of material property and morphological parameters on specimen-specific finite element models of porcine vertebral bodies. *J Biomech* 2007; **40**: 669–673.
52. Bourne BC, van der Meulen MCH. Finite element models predict cancellous apparent modulus when tissue modulus is scaled from specimen CT-attenuation. *J Biomech* 2004; **37**: 9–9.
53. Macneil JA, Boyd SK. Bone strength at the distal radius can be estimated from high-resolution peripheral quantitative computed tomography and the finite element method. *Bone* 2008; **42**: 1203–1213.
54. Dall'Ara E, Pahr D, Varga P, Kainberger F, Zysset P. QCT-based finite element models predict human vertebral strength in vitro significantly better than simulated DEXA. *Osteoporos Int* 2012; **23**: 563–572.
55. Yang X, Matsuda K, Bialek P, Jacquot S, Masuoka HC, Schinke T *et al.* ATF4 is a substrate of RSK2 and an essential regulator of osteoblast biology; implication for Coffin-Lowry Syndrome. *Cell* 2004; **117**: 387–398.
56. Edwards JR, Nyman JS, Lwin ST, Moore MM, Esparza J, O'quinn EC *et al.* Inhibition of TGF-β signaling by 1D11 antibody treatment increases bone mass and quality *in vivo*. *J Bone Miner Res* 2010; **25**: 2419–2426.
57. Mohammad KS, Chen CG, Balooch G, Stebbins E, McKenna CR, Davis H *et al.* Pharmacologic inhibition of the TGF-beta type I receptor kinase has anabolic and anti-catabolic effects on bone. *PLoS One* 2009; **4**: e5275.